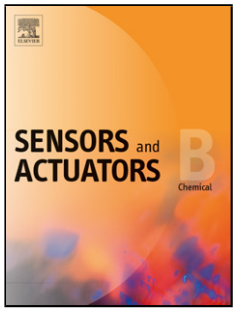

Title: Fluorescent Polymer Nanotubes as Bifunctional Materials for Selective Sensing and Fast Removal of Picric Acid

Authors: Meng Wang, Haitao Zhang, Lin Guo, Dapeng Cao

PII: S0925-4005(18)31379-0
DOI: https://doi.org/10.1016/j.snb.2018.07.132
Reference: SNB 25101

To appear in: *Sensors and Actuators B*

Received date: 25-5-2018
Revised date: 24-7-2018
Accepted date: 27-7-2018

Please cite this article as: Wang M, Zhang H, Guo L, Cao D, Fluorescent Polymer Nanotubes as Bifunctional Materials for Selective Sensing and Fast Removal of Picric Acid, *Sensors and amp; Actuators: B. Chemical* (2018), https://doi.org/10.1016/j.snb.2018.07.132

Fluorescent Polymer Nanotubes as Bifunctional Materials for Selective Sensing and Fast Removal of Picric Acid

Meng Wang, Haitao Zhang, Lin Guo, Dapeng Cao*

State Key Laboratory of Organic-Inorganic Composites, and Beijing Advanced Innovation Center for Soft Matter Science and Engineering, Beijing University of Chemical Technology, Beijing 100029, People's Republic of China

Graphical Abstract

TOC Graphics

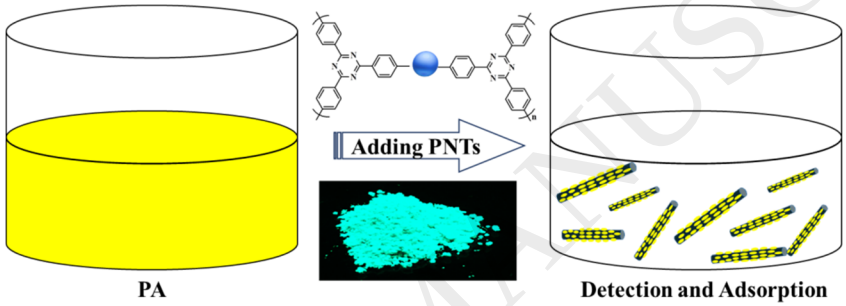

Highlights

- We have synthesized three porous organic polymer nanotubes (PNTs) with bifunctional applications
- The PNTs exhibit extremely high sensitivity and selectivity for fluorescent sensing picric acid (PA).
- The PNTs can adsorb PA rapidly, and the saturated capacity reaches 260 mg/g.
- The PNTs are excellent bifunctional materials for simultaneously sensing and removing PA.

Abstract

It is an urgent need to develop a bifunctional material for simultaneously sensing and removing explosives, because it is closely related to safety, environmental pollution and the health of human beings. Here, we have synthesized three porous organic polymer nanotubes (PNTs, PNT-4, PNT-5 and PNT-6) through Yamamoto coupling reaction. Results indicate that the three PNTs can be used not only as a fluorescent probe for high

selective and sensitive sensing of picric acid (PA) in real-time, but also as an excellent adsorbent for fast removal of PA from water. PNTs exhibit extremely high sensitivity for PA and the limit of detection concentration is lower than 2.36×10^{-9} M, and fluorescent quenching behavior of PNTs for PA can be well explained by the absorption competition quenching (ACQ) mechanism proposed in our previous literature. Moreover, the saturated adsorption capacities of PNT-4, PNT-5 and PNT-6 for PA reach 260.2, 200.5, and 178.8 mg/g, respectively. In short, the bifunctional properties of these PNTs for sensing and removing PA provide a useful strategy to find the PA pollution and further remove it in practical applications.

Keywords: Porous organic polymer nanotube; Bifunctional materials; Explosives; Luminescent probe; Absorption competition quenching mechanism; Adsorbents

1. Introduction

To promote the economic development and meet the needs of human beings, the chemical industries have brought severe environmental pollution problems.[1-3] The frequent occurrence of various pollution problems and poisoning events also seriously affect our life quality.[4, 5] Picric acid (PA) is one of the most dangerous nitroaromatic explosives, and its extensive applications not only lead to serious environment pollution, but also causes direct or indirect harm to the human body.[6-9] Short-term or long-term exposure to PA would yield significant health risks to animals and humans, such as anemia, carcinogenesis, abnormal liver function, cataracts, and so on.[10, 11] Therefore, to reduce pollution of PA for environment, it is a good strategy to develop bifunctional materials with the properties of simultaneously sensing and further removing PA.

In previous investigations, there are many reports on bifunctional materials for luminescent sensing and adsorption. Chen et.al[12] synthesized a metal organic framework (MOF) IFMC-10 with a BET surface area 185 $m^2 \cdot g^{-1}$, and it not only can be used as a luminescent probe for sensing Ln^{3+} but also can adsorb iodine. Cheng group[13] reported a microporous lanthanide MOF that can be used for selective sensing small-molecule pollutants and adsorption of CO_2. Duan et al.[14] reported a fluorescent MOF FITC@BTPY–NH_2 that can selectively sense Ag^+ and further adsorb Ag^+ in aqueous solution. Asif et.al[15] synthesized a hybrid material Fe_3O_4@Chitosan-pSDCalix, and it can be applied for the detection and removal of environmentally toxic Hg^{2+} ion from aqueous media. Wang group[16] prepared a thioether-based fluorescent covalent organic framework (COF) COF-LZU8 that can selectively detect and facilely remove mercury(II) in aqueous solutions. Yang et.al[17] reported a MOF-based magnetic adsorbent Fe_3O_4@SiO_2@UiO-67, and it can be used as bifunctional materials for detection and removal of organophosphorus pesticides. Besides bifunctional applications mentioned above, in fact, a lot of MOFs have been considered as fluorescent probes for sensing PA [18-22] and other toxic compounds.[23-25] For example, Qian group reported a water stable Eu-MOF that can be used to selectively detect PA.[26] Sanda et.al synthesized a Zn(II) based luminescent MOF for selectively detecting PA and palladium(II).[27] Suresh et al. used two dimensional Cd(II) MOF as an efficient luminescent sensor for detection of PA in aqueous media.[28-30] Although there are many studies on these materials as a fluorescent probe for sensing PA[31], the bifunctional materials with the properties of simultaneously sensing and adsorbing PA have not been reported previously yet.

Covalent organic polymers (COPs) have been widely used in gas adsorption and separation, bio-sensing, drug delivery, phototherapy, catalysts, optoelectronic materials fields due to its versatile elements, low density, stable structure, controllable functionalization modification, intrinsic porosity and large specific surface area, etc.[32-37] Xiang et.al [38] synthesized a series of COP materials for carbon capture, and the BET specific surface areas can be tuned by tailoring the length and geometry of building blocks. Cao group reported a series of fluorescent COP materials that can be used to detect nitro explosives[39], metal ions[40], small organic molecules[41] and toxic gases[42]. Liu group synthesized two fluorescent conjugated microporous polymers DTF and TTF, and DTF can be used as fluorescent probe to selectively detect PA.[43] Guo et.al synthesized nanoscale conjugated microporous polymer (NCMP) capsules that have a tunable NIR absorption ability, which can generate heat upon exposure to 808 nm light and cause thermal ablation of HeLa cells.[44] Wang et al. used conjugated microporous polymer nanosheets (CMPNs) for overall water splitting under visible light (400 nm) via a four-electron pathway.[45] The excellent fluorescent property and BET tunable property make COP materials good candidates for the bifunctional application in detection and adsorption of explosives.

In this work, we synthesize three porous organic polymer nanotubes (PNT-4, PNT-5 and PNT-6) by using Ni-catalyzed Yamamoto coupling reaction, and further investigate their fluorescent and adsorption properties for PA to explore its possibility as bifunctional materials. We also study the influence of the length of the benzene ring for the fluorescent

and adsorption properties of PNTs. Finally, some conclusions are drawn and some discussions are addressed.

2. Experimental Section

2.1 Synthesis of polymer nanotubes

The PNTs (PNT-4 ~ PNT-6) were synthesized by Yamamoto-type Ullmann cross-coupling reaction, in which TBT was used as one monomer and DB, 2DB, 3DB as another monomer. The synthesis route of the PNTs was shown in Scheme 1, and the specific experimental processes were presented as follows. First, cod (0.505 mL, 3.96 mmol, dried with CaH_2), $Ni(cod)_2$ (1.125 g, 4.09 mmol), and 2,2'-bipyridyl (0.640 g, 4.09 mmol) were added to dry DMF (65 mL) in the pressure flask, and then the mixture was stirred at 40 °C until completely dissolved, purple solutions were obtained in this process. Second, the monomer TBT (0.172 g, 0.314 mmol) and DN (0.111 g, 0.471 mmol) were added to the above-mentioned pressure flask, and the pressure flask was put on the heating agitator and kept at 80 °C for 12 h. All above experiments were carried out in a glove box under an argon atmosphere. After the reaction was completed, the mixture was cooled down to room temperature. Subsequently concentrated HCl was dropwise added into the above purple suspension, until the color of the solution changed from purple into light green transparent. After filtration, the residues were washed by $CHCl_3$ (5×15 mL), THF (5×15 mL) and H_2O (5×15 mL), respectively. Finally, the solid residues were dried in a vacuum oven of 140 °C for 24 h, and the dried sample (namely PNT-4) was placed in containers and stored in a desiccator.

The detailed synthesis procedure and reaction conditions of PNT-5 and PNT-6 are same with PNT-4, and the only difference is that the monomer DB was replaced by the monomers of 2DB and 3DB, respectively.

2.2 Fluorescence and adsorption measurements

The fluorescent spectra of the powder monomers and three PNTs were measured by fluorescence spectrophotometer. The photoluminescence (PL) properties of the three PNT materials in solvent were investigated at room temperature. The explosives used in the fluorescent detecting experiment include picric acid (PA), nitrobenzene (NB), m-dinitrobenzene (m-DNB), p-nitrophenol (p-NP), 4-nitrobenzoic acid (p-NBA), o-nitrophenol (o-NP), m-nitrophenol (m-NP), 3-nitrotoluene (3-NT), phenol, p-benzenediol (p-BD), 2,4-dinitrotoluene (2,4-DNT), and 4-nitrotoluene (4-NT). The explosive solutions (1.0 mM) were prepared in ethanol and water. The PNT materials (1 mg/10 mL) were dispersed in ethanol solvent through ultrasound. It should be noted that considering the nontoxicity of solvents in practical applications, we selected ethanol as solvent rather than dichloromethane and THF and DMF with toxicity as solvents. The PL emission spectra of the PNT-EtOH suspensions (1 mg/10 mL) were recorded before and after adding a series of explosives with the same concentration (10^{-5} M), which contains PA, NB, m-DNB, p-NP, p-NBA, o-NP, m-NP, 3-NT, phenol, p-BD, 2,4-DNT, and 4-NT. To explore the sensitivity of PNTs for sensing PA, the PL emission spectra of the PNT-EtOH suspensions (1 mg/10 mL) were investigated by testing the fluorescent intensity changes in presence of PA with different concentrations of 3×10^{-7}, 6×10^{-7}, 9×10^{-7}, 10^{-6}, 2×10^{-6}, 4×10^{-6}, 8×10^{-6}, and 10^{-5} M. To examine the selectivity of PNTs for sensing PA and the effects of

other explosives on the selectivity of PNTs for PA, PL emission spectra of the PNT suspensions (1 mg/10 mL) were investigated by testing the fluorescent intensity changes before and after adding different combinations of explosives, and the PL spectra of in the presence of all other explosives before and after adding PA are also recorded, where the concentration of the explosives is 10^{-5} M.

Adsorption experiments of PNTs for PA were also performed to explore its bifunctional applications as adsorbent. First, 200 ppm PA aqueous solution was prepared. 50 mg PNTs (PNT-4, PNT-5, and PNT-6) were added into 200 mL PA (200 ppm) solutions and stirred, respectively. Then, the samples were took out for measurements at predetermined times, and millipore membranes were used to filter the solution and the concentrations of remaining PA were determined by the UV–Vis spectrophotometer (TU-1901). Finally, the adsorption capacity and removal percent of PNTs for PA were obtained.

3. Results and Discussion

The successful synthesis of the three PNTs (PNT-4 ~ PNT-6) by Yamamoto-type coupling reaction can be confirmed by FTIR spectra (Figure 1a ~ 1c). The absence of C-Br stretching peak around 512 cm^{-1} in the FTIR spectra marked by yellow rectangular box indicates that the Br functional groups in the monomers have been consumed completely by phenyl-phenyl coupling. The PXRD pattern indicates that all PNTs are amorphous structure (Figure S1). TGA analysis under N_2 (Figure 1d) indicates that all these three PNTs possess good thermal stability, and the three PNTs have only 5% mass loss when they are heated to 610 °C. The porosity of these PNTs was characterized by N_2 adsorption

at T=77K, and the N_2 adsorption and desorption isotherms were shown in Figure 1e. The BET specific surface areas of PNT-4, PNT-5 and PNT-6 are 1311.54, 817.32 and 433.24 m^2/g, respectively. It can be found that the BET of the PNTs decreases with the increasing of the length of monomers (DB, 2DB and 3DB), due to the interpenetration between the benzene rings with the increase in the length of the benzene ring, just as shown in scheme 1. The pore size distributions are shown in Figure 1f, where the pore size of PNT-4, PNT-5, and PNT-6 are all distributed in the range of mesoporous (2-50 nm), and the detailed pore volume and pore size of the three PNTs are listed in Table S1. Figure 1g ~ 1i shows the SEM images of PNT-4, PNT-5 and PNT-6, respectively, which clearly present apparent nanotube structure.

The solid-state PL emission spectra of the three PNTs with excitation $\lambda ex = \lambda ex_{max}$ at room temperature were shown in Figure 2a ~ 2c, and the detailed excitation and emission spectra of the PNTs were presented in Table S2. The emission peaks of PNT-4, PNT-5 and PNT-6 are 457 nm, 456 nm and 460 nm, respectively. The PL emission spectra of the corresponding monomers were shown in Figure S2. Compared to the monomers (TBT, DB, 2DB and 3DB), the maximum fluorescent intensities of all three PNTs are enhanced significantly, especially for PNT-4. This fluorescence enhancement phenomenon can be explained as follows. One is attributed to the π-π conjugate bonds produced by the phenyl-phenyl coupling reaction, which increases the π conjugate degree of the PNTs to improve the fluorescence intensity. On the other hand, the PNT materials are more stable compared to the monomers and could therefore reduce the energy consumption during vibrational relaxation, which is the same as the AIE effect.[46, 47] Moreover, we notice that the

luminescence intensity of these three PNTs decreases with the increase of the length of the monomers, which can be rationally explained by the interpenetration between the benzene rings that affects the electron cloud density and π-conjugation degree. The specific fluorescent and porous properties of the PNTs allows us to consider it as a bifunctional material for fluorescent sensing and adsorbent of explosives.

First, we investigated the PNTs (PNT-4, PNT-5 and PNT-6) properties as a fluorescent probe for sensing explosives through a series of fluorescent experiments by adding successive aliquots of explosives (including p-BD, phenol, p-NP, m-BD, p-NBA, 4-NT, 2,4-DNT, m-NP, m-NT, m-DNB, p-DNB, o-NP, PA). The PL emission spectra and the relative fluorescent intensity of PNTs upon adding various explosives were shown in Figure S3 and Figure 2d ~ 2f, where the fluorescent intensity of PNTs exhibits different quenching degrees after adding explosives. Interestingly, the fluorescent intensity of PNTs were almost quenched completely after adding PA, while the fluorescent intensity of PNTs have no obvious change after adding other explosives (p-BD, phenol, p-NP, m-BD, p-NBA, 4-NT, 2,4-DNT, m-NP, m-NT, m-DNB, p-DNB, and o-NP), indicating that all three PNTs exhibit extremely high selectivity for sensing PA. The fluorescent photographs of PNT-EtOH suspensions before and after adding explosives under an UV lamp were shown in Figure 2g and Figure S4, where the quenching effect of PNTs for PA can be observed clearly by naked eyes.

To examine the crossover effect of other explosives, we also performed a series of competitive experiments to further explore the selectivity of all three PNTs for PA in the presence of other explosives. The fluorescent intensity and PL emission spectra of PNTs

in different kinds of explosive mixtures (with PA and without PA) were recorded. As shown in Figure 3 and Figure S5 ~ S8, the fluorescent intensity and PL emission spectra of PNTs did not change significantly after adding other explosives with different combinations (eg. p-BD, phenol, p-NP, m-BD, p-NBA, 4-NT, 2,4-DNT, m-NP, m-NT, m-DNB, p-DNB, and o-NP), while the fluorescent intensity was almost quenched completely as long as PA was added to the above solutions, indicating that all the PNTs have extremely high selectivity for sensing PA even in the presence of all other explosives.

In addition, we also explored the sensitivity of PNTs as fluorescent probes for sensing PA by adding different concentrations of PA via real-time fluorescence response. Figure 4(a) ~ 4(c) show the corresponding fluorescence spectra of PNTs, and the peak position of the emission spectra was not changed after adding different concentrations of PA. Moreover, the fluorescent intensity of the PA-incorporated PNTs is largely dependent on the concentration of the PA, and the fluorescent intensity of the PA-incorporated PNTs gradually decreased with the increase of the concentrations of PA. To qualitatively describe the quenching effect of PNTs for PA, we calculated the quenching coefficient by using the Stern-Volmer equation: $I_0/I=1+Ksv\cdot[M]$, where I_0 is the initial fluorescent intensity of PNTs without any analyte, I is the fluorescent intensity of PNTs after adding the analyte with the concentration of [M], and Ksv is the quenching coefficient of PNTs for PA. As shown in Figure 4(d) and 4(f), a good linear Stern-Volmer relationship was observed for PNTs, and the quenching coefficients of PNT-4, PNT-5 and PNT-6 for PA were 621901, 507800, 238278, respectively, indicating that PNTs also have an extremely high sensitivity for detecting PA.

All above results indicate that the three PNTs exhibit not only excellent selectivity but also high sensitivity for sensing PA. Here we also compared the Ksv and further calculated the quantitative selectivity of PNTs for sensing PA, i.e. $S=I_0/I_{PA}$, where I_0 is the fluorescence intensity of PNTs, I_{PA} is the fluorescence intensity of PNTs after adding PA. As shown in Table 1, the S and Ksv follow an order of PNT-4 > PNT-5 > PNT-6, which is obviously the same as BET SSAs, possibly because that PA is more easily contact with the surface of PNTs with higher BET. In addition, the limit of detection (LOD) concentration of the PNTs for fluorescent sensing PA was calculated by $3\sigma/k$ (k: slope, σ: standard deviation), and the LODs of PNT-4, PNT-5 and PNT-6 are about 2.36×10^{-9} M, 3.12×10^{-9} M, and 5.52×10^{-9} M, respectively, which are lower than most previously reported fluorescent materials for detecting PA.[48-50] In addition, we also explored the recycling utilization of PNTs. As shown in Figure S9, all of these three PNTs have good recyclability and can still maintain good fluorescent detection performance after repeated utilization for 6 times, which provides promising potential for the practical application of PNTs as a bifunctional material.

The fluorescent quenching mechanism of the PNTs for selective detecting PA was also studied by the UV-Vis absorption spectra of the PNT suspensions and explosives (see Figure 5), and absorption competition quenching (ACQ) mechanism was applicable.[51] Compared to all other explosives, PA has a higher absorption peak and a larger absorption spectrum overlap with PNTs, indicating that a strong absorption competition of the light source energy between PA and PNTs existed. The PA filtered the light energy absorbed by the PNTs so that the energy absorbed by PNTs decreased and the electrons cannot be

transferred to the excited state, thus the fluorescence of PNTs quenched. Figure 5d~5f show the absorption spectra of PA with different concentrations, in which the absorbance of the PA gradually increases with the increase of PA concentration, and the overlap degree between PA and PNTs increases apparently. This observation coincides with the order of fluorescence quenching of PNTs, which also further proves the above-mentioned ACQ mechanism.

PNTs not only possess high intrinsic fluorescent intensity, but also exhibit good porosity. As porous materials with high BET surface, these PNTs also hold the ability to adsorb analyte. Therefore, we also studied the adsorption property of these PNTs for PA. Adsorption capacity (Ac, mg/g) is one of the most important characteristics of porous materials as adsorbent, and it can be calculated by the equation: $Ac = (c_i-c_t)/M$, where Ac is the amount of PA adsorbed on per gram adsorbent at contact time t, c_i (mg/L) is the initial concentration and c_t is the concentration of PA in the solution at contact time t, M (g/L) is the adsorbent concentration in per liter solution. The experiments were carried out by adding 50 mg PNTs to 200 mL solutions that containing 200 ppm of PA at room temperature with contact time ranging from 1 to 140 mins, where the amount of PA was excessed. Figure 6 shows the instantaneous adsorption capacities of PNT-4, PNT-5 and PNT-6 for PA in different contact time, which are typical Langmuir isotherms. Interestingly, it needs only several mins to reach saturation adsorption of PA in the PNTs, which means that the PNTs can fast remove the PA from water. The equilibrium adsorption capacities of PNT-4, PNT-5 and PNT-6 are 260.2, 200.5 and 178.8 mg/g, respectively (see Table 1), which are much higher than many other reported adsorbents for

adsorption of PA[52-55]. Moreover, the order of adsorption capacity of PNTs for PA also closely fellows the one of BET SSAs, because the BET SSA of a porous material is the key to adsorption capacity of PA. The adsorption efficiency of PNTs also can be easily identified by naked eyes, and the solution with PA becomes clarification after adding excessive PNTs (see inset in Figure 6). These results indicate that PNTs can effectively adsorb and remove PA from water. Moreover, this adsorption phenomenon can be explained by the Zeta potential. Zeta potentials of PNT-4, PNT-5 and PNT-6 are 10.9, 10.3 and 10.2 mV, respectively, while the Zeta potential of PA is -8.85 mV. The opposite of the potential indicates that there exist interaction between PNTs and PA, which is favorable for PA adsorbed by PNTs.

4. Conclusions

In conclusion, three fluorescent PNTs (PNT-4, PNT-5 and PNT-6) have been synthesized successfully by Yamamoto coupling reaction. Results indicated that the three PNTs can be used as fluorescent probes for highly selective and sensitive detecting PA in real-time, and the LOD concentration was lower than 2.36×10^{-9} M. Absorption competition quenching (ACQ) mechanism can explain the behavior of PNTs for fluorescent sensing PA. In addition, the adsorption isotherm of PNTs for PA was also measured, and the saturated adsorption capacities of PNT-4, PNT-5 and PNT-6 for PA were 260.2, 200.5 and 178.8 mg/g, respectively, meaning that PNTs can effectively adsorb and remove PA from water. In short, these PNTs not only can be used as fluorescent probes for highly selective and sensitive sensing PA, but also can be used as adsorbents

for the adsorption of PA. These excellent bifunctional properties of PNTs provide the possibility for practical applications.

Acknowledgements

This work is supported by National Science Fund for Distinguished Young Scholars (No. 21625601) and Outstanding Talent Fund from BUCT.

References

[1] U. Biermann, W. Friedt, S. Lang, W. Lühs, G. Machmüller, J.O. Metzger, G.K.M. Rüsch, H.J. Schäfer, M.P. Schneider, Angew. Chem. Int. Edit. 31 (2010) 253-289.

[2] W. Li, C. Lu, Y. Ding, Y.W. Zhang, Appl. Energ. 204 (2017) 509-524.

[3] S.M. Gallego, M.P. Benavídes, M.L. Tomaro, Plant Sci. 121 (1996) 151-159.

[4] M.H. Huesemann, Ecol. Econ. 37 (2001) 271-287.

[5] A.F. Manini, L.S. Nelson, A.H. Skolnick, W. Slater, R.S. Hoffman, J. Med. Toxicol. 6 (2010) 106-115.

[6] K. Gao, Y. Guo, Q. Niu, L. Han, L. Zhou, L. Wang, Sensor. Actuat. B Chem. 262 (2018) 298-305.

[7] M. Nipper, R.S. Carr, J.M. Biedenbach, R.L. Hooten, K. Miller, Mar. Pollut. Bull. 50 (2005) 1205-1217.

[8] M. Nipper, Y. Qian, R.S. Carr, K. Miller, Chemosphere 56 (2004) 519.

[9] X. Tian, X. Qi, X. Liu, Q. Zhang, Sensor. Actuat. B Chem. 229 (2016) 520-527.

[10] Z.H. Fu, Y.W. Wang, Y. Peng, Chem. Commun. 53 (2017) 10524-10527.

[11] J.H. Qin, H.R. Wang, M.L. Han, X.H. Chang, L.F. Ma, Dalton T. 46 (2017) 15434-15442.

[12] L. Chen, K. Tan, Y.-Q. Lan, S.-L. Li, K.-Z. Shao, Z.-M. Su, Chem. Commun. 48 (2012) 5919-5921.

[13] H. Li, W. Shi, K. Zhao, Z. Niu, H. Li, P. Cheng, Chem. A Eur .J. 19 (2013) 3358-3365.

[14] L. Zhang, Y. Jian, J. Wang, C. He, X. Li, T. Liu, C. Duan, Dalton T. 41 (2012) 10153-10155.

[15] A.A. Bhatti, M. Oguz, M. Yilmaz, Appl. Surf. Sci. 434 (2018) 1217-1223.

[16] S.Y. Ding, M. Dong, Y.W. Wang, Y.T. Chen, H.Z. Wang, C.Y. Su, W. Wang, J. Am. Chem. Soc. 138 (2016) 3031-3037.

[17] Q. Yang, J. Wang, X. Chen, W. Yang, H. Pei, N. Hu, Z. Li, Y. Suo, T. Li, J. Wang, J. Mater. Chem. A 6 (2018) 2184-2192.

[18] P. Das, S. Mandal, J. Mater. Chem. C 6 (2018) 3288-3297.

[19] Y. Han, Y. Chen, J. Feng, J. Liu, S. Ma, X. Chen, Anal. Chem. 89 (2017) 3001-3008.

[20] W. Huang, E. Smarsly, J. Han, M. Bender, K. Seehafer, I. Wacker, R.R. Schrã¶Der, U.H. Bunz, Acs Appl. Mater. Inter. 9 (2017) 3068-3074.

[21] M. Kaur, S.K. Mehta, S.K. Kansal, Sensor. Actuat. B Chem. 245 (2017) 938-945.

[22] J. Li, J. Li, Inorg. Chem. Commun. 89 (2018) 51-54.

[23] L. Guo, M. Wang, D. Cao, Small 14 (2018) 1703822.

[24] M. Wang, L. Guo, D. Cao, Anal. Chem. 90 (2018) 3608-3614.

[25] M. Wang, L. Guo, D. Cao, Sens. Actuat. B- Chem. 256 (2018) 839-845.

[26] T. Xia, F. Zhu, Y. Cui, Y. Yang, Z. Wang, G. Qian, J. Solid State Chem. 245 (2017) 127-131.

[27] S. Sanda, S. Parshamoni, S. Biswas, S. Konar, Chem. Commun. 51 (2015) 6576-6579.

[28] Y. Rachuri, B. Parmar, K.K. Bisht, E. Suresh, Dalton T. 45 (2016) 7881-7892.

[29] Y. Rachuri, B. Parmar, K.K. Bisht, E. Suresh, Cryst. Growth. Des. 17 (2017) 1363-1372.

[30] B. Parmar, Y. Rachuri, K.K. Bisht, R. Laiya, E. Suresh, Inorg. Chem. 56 (2017) 2627-2638.

[31] Z.Q. Shi, Z.J. Guo, H.G. Zheng, Chem. Commun. 51 (2015) 8300-8303.

[32] Z. Xiang, X. Zhou, C. Zhou, S. Zhong, X. He, C. Qin, D. Cao, J. Mater. Chem. 22 (2012) 22663-22669.

[33] Z. Xiang, D. Cao, L. Huang, J. Shui, M. Wang, L. Dai, Adv. Mater. 26 (2014) 3315-3320.

[34] L. Yang, D. Cheng, H. Xu, X. Zeng, X. Wan, J. Shui, Z. Xiang, D. Cao, PNAS, 115 (2018) 6626-6631.

[35] L. Guo, D. Cao, J. Mater. Chem. C 3 (2015) 8490-8494.

[36] J.X. Jiang, Y. Li, X. Wu, J. Xiao, D.J. Adams, A.I. Cooper, Macromolecules 46 (2013) 8779-8783.

[37] S. Yao, X. Yang, M. Yu, Y. Zhang, J.X. Jiang, J. Mater. Chem. A 2 (2014) 8054-8059.

[38] Z. Xiang, R. Mercado, J.M. Huck, H. Wang, Z. Guo, W. Wang, D. Cao, M. Haranczyk, B. Smit, J. Am. Chem. Soc. 137 (2015) 13301-13307.

[39] N. Sang, C. Zhan, D. Cao, J. Mater. Chem. A 3 (2015) 92-96.

[40] M. Wang, G. Lin, D. Cao, Sci. China Chem. 60 (2017) 1090-1097.

[41] L. Guo, X. Zeng, D. Cao, Sensor. Actuat. B Chem. 226 (2016) 273-278.

[42] L. Guo, M. Wang, X. Zeng, D. Cao, Mater. Chem. Front. 1 (2017) 2643-2650.

[43] T.-M. Geng, S.-N. Ye, Y. Wang, H. Zhu, X. Wang, X. Liu, Talanta 165 (2017) 282-288.

[44] J. Tan, J. Wan, J. Guo, C. Wang, Chem. Commun. 51 (2015) 17394-17397.

[45] L. Wang, Y. Wan, Y. Ding, S. Wu, Y. Zhang, X. Zhang, G. Zhang, Y. Xiong, X. Wu, J. Yang, Adv. Mater. 29 (2017) 1702428-1702436.

[46] Q. Zeng, Z. Li, Y. Dong, C. Di, A. Qin, Y. Hong, L. Ji, Z. Zhu, C.K. Jim, G. Yu, Chem. Commun. 1 (2007) 70-72.

[47] D. Li, J. Liu, R.T. Kwok, Z. Liang, B.Z. Tang, J. Yu, Chem. Commun. 48 (2012) 7167-7169.

[48] S.S.R. Dasary, A.K. Singh, K.S. Lee, H. Yu, P.C. Ray, Sensor. Actuat. B Chem. 255 (2017) 1646-1654.

[49] W. Che, G. Li, X. Liu, K. Shao, D. Zhu, Z. Su, M.R. Bryce, Chem. Commun. 54 (2018) 1730-1733.

[50] L.L. Wen, X.G. Hou, G. Shan, W.L. Song, S.R. Zhang, H. Sun, Z.M. Su, L.L. Wen, X.G. Hou, G. Shan, J. Mater. Chem. C 5 (2017) 10847-10854.

[51] L. Guo, X. Zeng, J. Lan, J. Yun, D. Cao, Chemistryselect 2 (2017) 1041-1047.

[52] D. Mohan, A. Sarswat, V.K. Singh, M. Alexandre-Franco, C.U.P. Jr, Chem. Eng. J. 172 (2011) 1111-1125.

[53] H. Parham, B. Zargar, M. Rezazadeh, Mater. Sci. Eng. C 32 (2012) 2109-2114.

[54] H. Sepehrian, J. Fasihi, M.K. Mahani, Ind. Eng. Chem. Res. 48 (2009) 6772-6775.

[55] H. Uslu, G. Demir, J. Chem. Eng. Data 55 (2010) 3290-3296.

Author Biographies

Meng Wang is a PhD candidate under the supervision of Professor Daepng Cao at the Beijing University of Chemical Technology. Her main research interests are the design, synthesis and applications of luminescent porous organic materials as luminescent probes for sensing different ions and nitro explosives. She has published several articles in journals like *Anal. Chem.*, *Small* and *Sens. Actuat. B- Chem.*, etc.

Haitao Zhang is a Master student under the supervision of Professor Daepng Cao at the Beijing University of Chemical Technology. Her main research interests are the synthesis of porous organic materials and its application in the separation and removal of pollutants in water.

Lin Guo is a PhD candidate under the supervision of Professor Daepng Cao at the Beijing University of Chemical Technology. Her main research interests are the synthesis of luminescent porous organic materials and its application as luminescent probes. She has published several articles in journals like *J. Mater. Chem. C*, *Small* and *Sens. Actuat. B-Chem.*, etc.

Dapeng Cao is a Professor and Director of the Division of Molecular and Materials Simulation, State Key Laboratory of Organic-Inorganic Composites at Beijing University of Chemical Technology (BUCT) (2005-). He received his Ph D from BUCT in 2002, and was a research scientist at NanoMaterials Technology Pte Ltd in Singapore (2002-2003) and a postdoctoral researcher at the University of California at Riverside (2003-2005). His research interests are focused on the designed synthesis and applications of functional materials, including porous luminescent polymers and energy catalysis materials. Currently, he is a Fellow of the Royal Society of Chemistry (FRSC). He has published more than two hundred articles in journals such as *Nature Catalysis*, *PNAS*, *J. Am. Chem. Soc.*, *Angew. Chem. Int. Ed.*, etc.

Figures

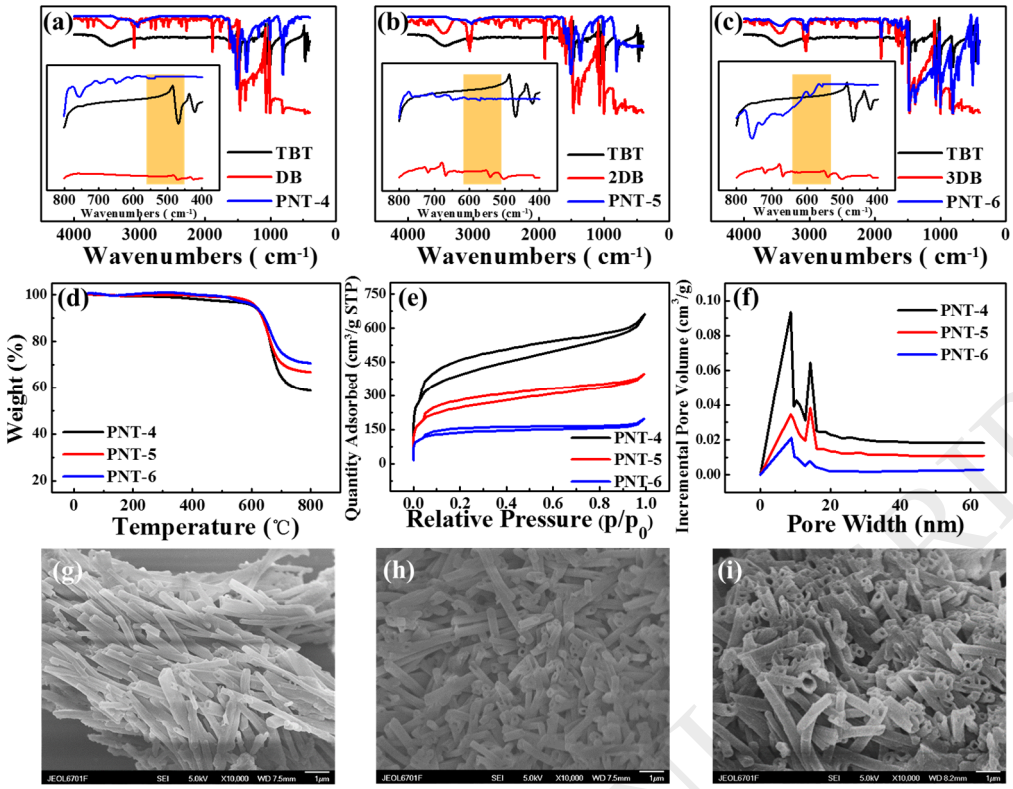

Figure 1 (a) FTIR spectra of the PNT-4 (blue line), TBT (black line) and DB (red line) from 400-4000 cm^{-1} and 400-800 cm^{-1} (the inset); **(b)** FTIR spectra of the PNT-5 (blue line), TBT (black line) and 2DB (red line) from 400-4000 cm^{-1} and 400-800 cm^{-1} (the inset); **(c)** FTIR spectra of the PNT-6 (blue line), TBT (black line) and 3DB (red line) from 400-4000 cm^{-1} and 400-800 cm^{-1} (the inset); **(d)** TGA curves of PNT-4 (black line), PNT-5 (red line), PNT-6 (blue line); **(e)** N_2 adsorption isotherms at T =77K. Black, red and blue line represent adsorption and desorption for PNT-4, PNT-5 and PNT-6, respectively; **(f)** Nonlocal density functional theory (NLDFT) pore size distributions of the PNTs by incremental pore volume; **(g) ~ (i)** SEM images of PNT-4, PNT-5 and PNT-6, respectively.

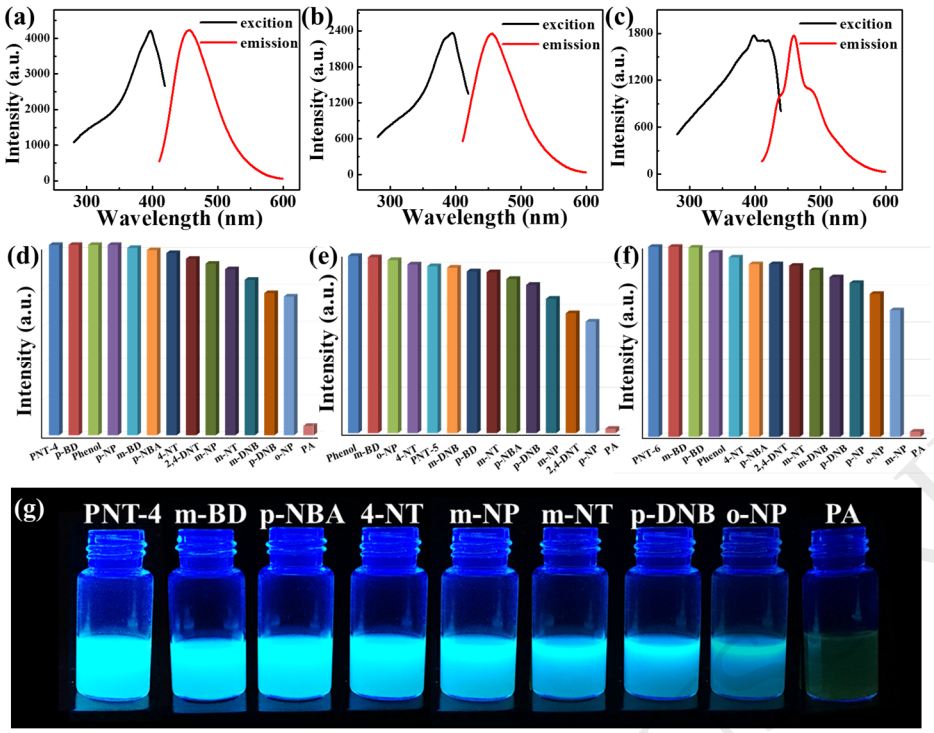

Figure 2 (a) ~ **(c)** are the excitation (black line) and PL emission spectra (red line) of the solid-state PNT-4, PNT-5 and PNT-6, respectively; **(d)** ~ **(f)** are the fluorescent intensity of PNTs (PNT-4, PNT-5 and PNT-6) interacting with different explosives in 10^{-5} M ethanol solutions, where the widths of the excitation slit are 5 nm and emission slit is 10 nm for PNTs; **(g)** The PL photographs of PNT-4 before and after adding different explosives, where PL is excited under λex=365 nm using a portable UV lamp.

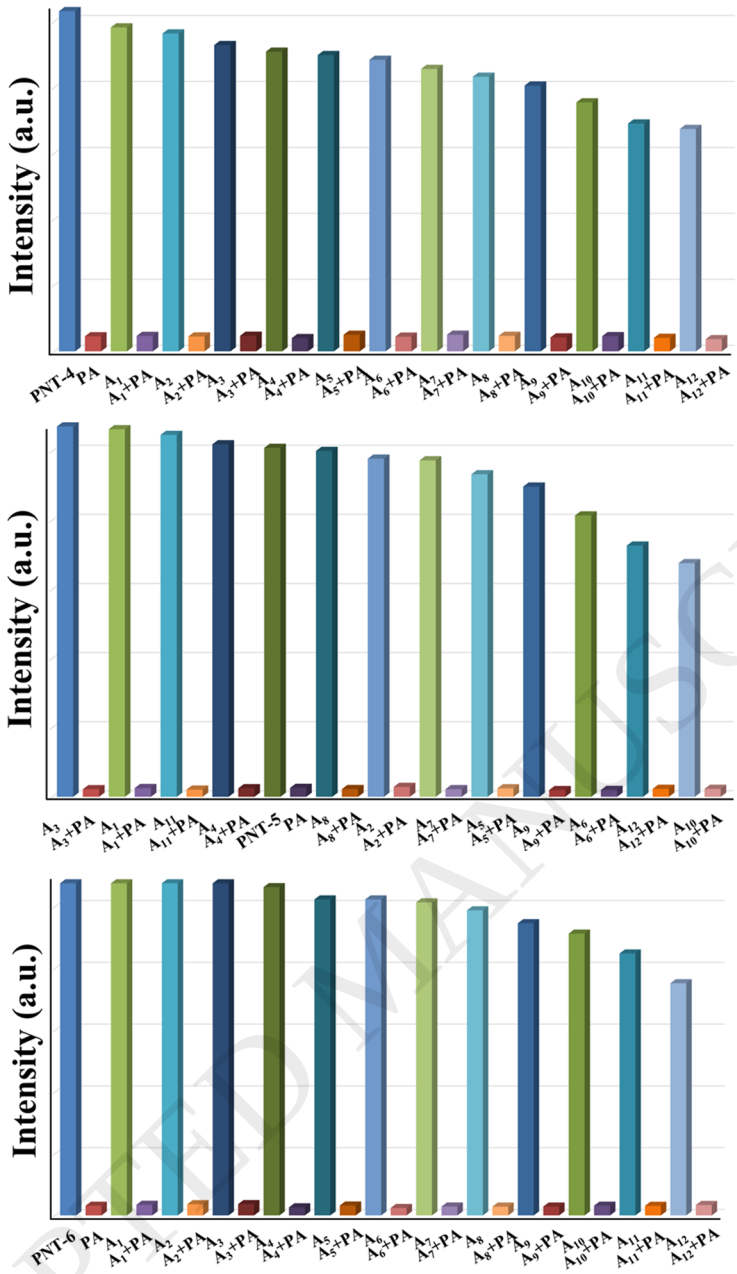

Figure 3 Selectivity of PNTs for sensing PA. **(a)** PNT-4; **(b)** PNT-5; **(c)** PNT-6. A_1: p-BD; A_2: phenol; A_3: p-NP; A_4: m-BD; A_5: p-NBA; A_6: 4-NT; A_7: 2,4-DNT; A_8: m-NP; A_9: m-NT; A_{10}: m-DNB; A_{11}: p-DNB; A_{12}: o-NP.

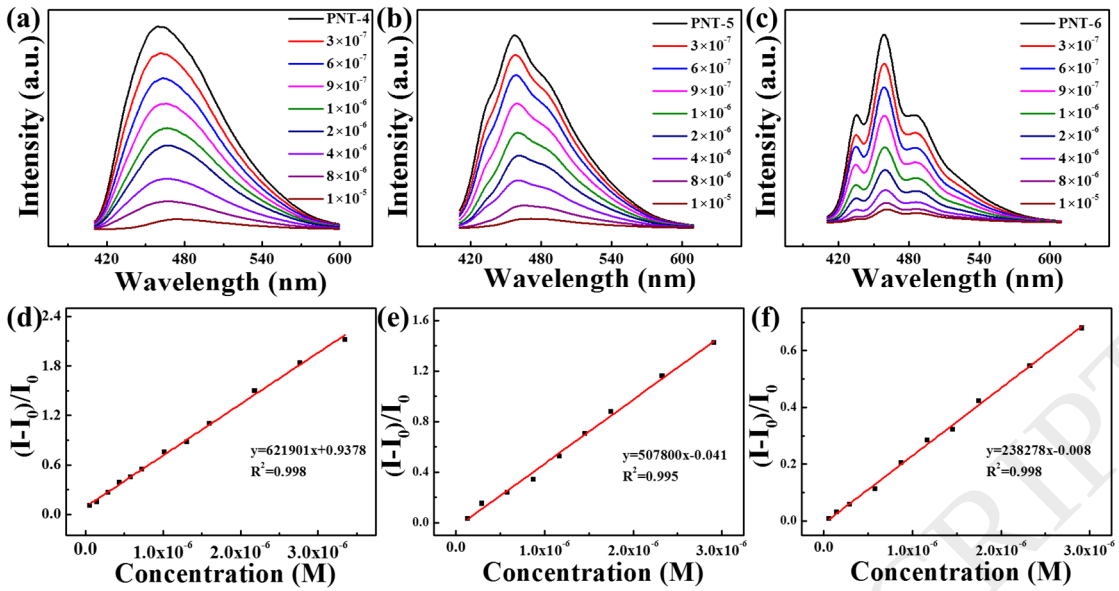

Figure 4 (a) ~ (c) are PL emission spectra of PNT-4, PNT-5 and PNT-6 dispersed in solvents after adding different concentrations of PA, respectively. From top to bottom, the concentration of PA are 0, 3×10^{-7}, 6×10^{-7}, 9×10^{-7}, 10^{-6}, 2×10^{-6}, 4×10^{-6}, 8×10^{-6} and 10^{-5} M, respectively; **(d) ~ (f)** are Stern–Volmer plots of PNT-4, PNT-5 and PNT-6 for sensing PA, respectively.

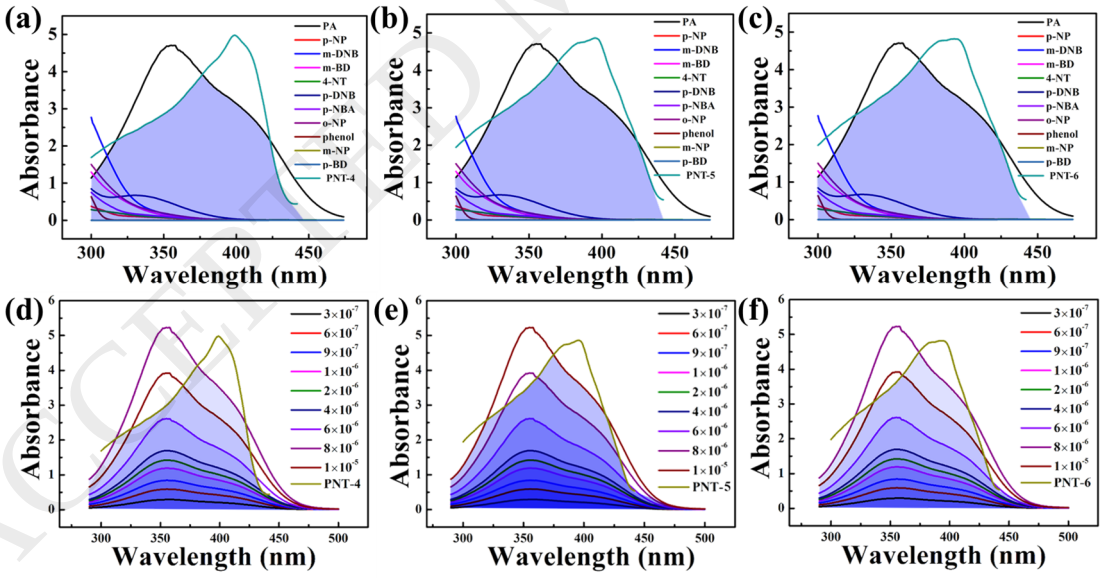

Figure 5 (a) ~ (c) Absorption spectra of explosives and PNTs (PNT-4, PNT-5 and PNT-6) in ethanol solutions, and the shaded area indicates the overlap of the absorption spectra of the PNTs and PA; **(d) ~ (f)** Absorption spectra of PNTs (PNT-4, PNT-5 and PNT-6) and different concentrations of PA in ethanol solutions. From top to bottom, the concentration of PA are 3×10^{-7},

6×10^{-7}, 9×10^{-7}, 10^{-6}, 2×10^{-6}, 4×10^{-6}, 8×10^{-6} and 10^{-5} mol·L^{-1}, respectively, and the shaded area indicates the overlap of the absorption spectra of the PNTs and PA.

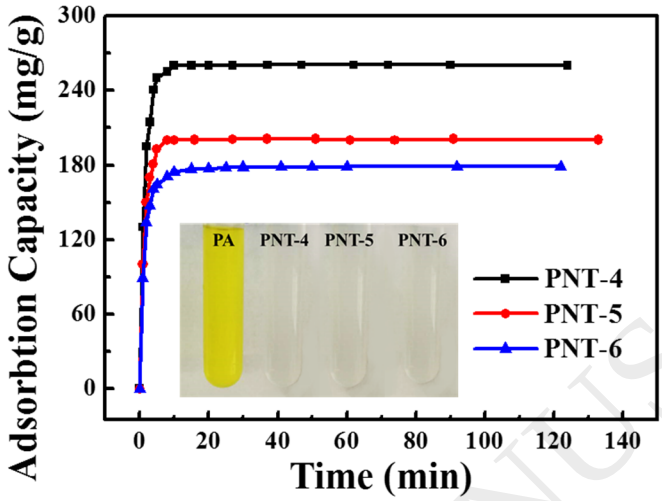

Figure 6 The kinetic data diagram for PA absorbed by PNTs. (Adsorption conditions: adsorbent dose = 5 mg, *V*=100 mL, *T* = 298 K, contact time = 2.5 h). The inset presents a photograph of the PA solutions before and after adsorbing by PNTs.

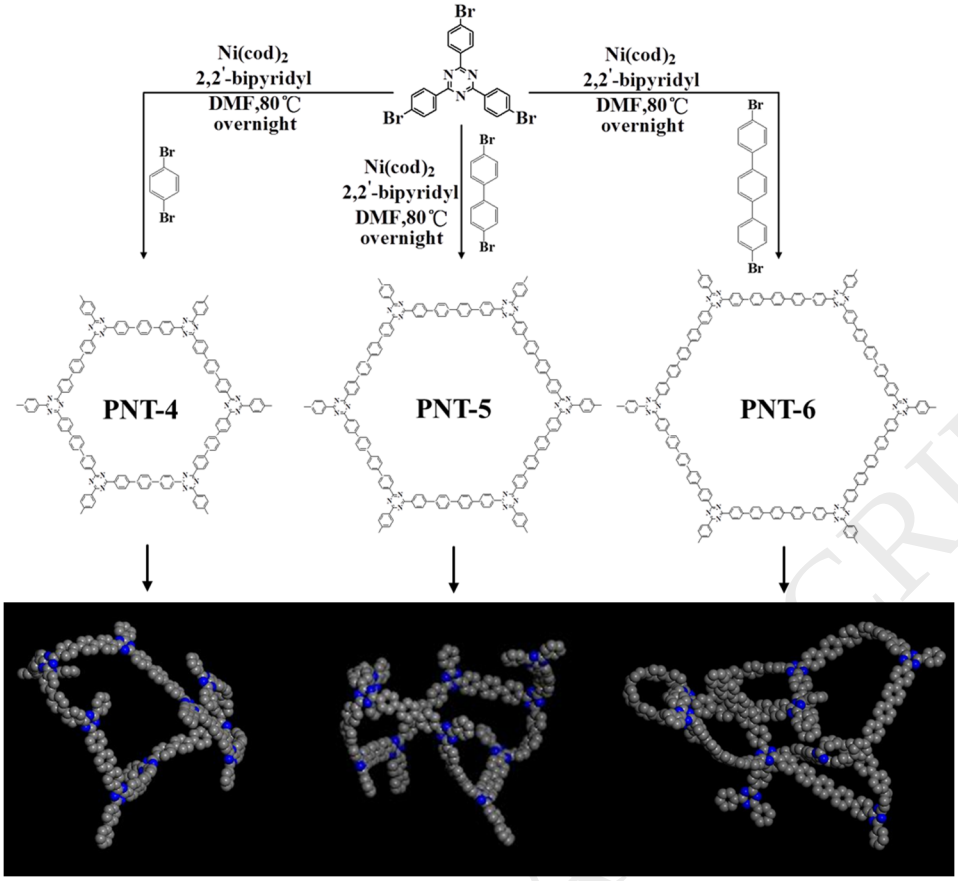

Scheme 1 Synthetic routes of PNTs by Ni-catalyzed Yamamoto-type Ullmann cross-coupling reaction. The actual structures of these PNTs may be more complex than represented.

Table 1 The BET specific surface areas of the PNTs, and the selectivity and adsorption capacity of PNTs for PA.

Material	BET SSAs [m^2/g]	S	Ksv	Adsorption Capacity (mg/g)
PNT-4	1311.54	48.26	621901	260.2
PNT-5	817.32	38.77	507800	200.5
PNT-6	433.24	30.39	238278	178.8